Fiber waviness in nanotube-reinforced polymer composites: I. Modulus predictions using effective nanotube properties

F.T. Fisher, R.D. Bradshaw[*] and L.C. Brinson[**]

Department of Mechanical Engineering, Northwestern University

2145 Sheridan Road, Evanston, IL 60208, USA

Substantial improvements in the mechanical behavior of polymers have been attained through the addition of small amounts of carbon nanotubes as a reinforcing phase, suggesting the possibility of new, extremely lightweight carbon nanotube-reinforced polymers with mechanical properties comparable to those of traditional carbon-fiber composites. Motivated by micrographs showing that embedded nanotubes often exhibit significant curvature within the polymer, we have developed a model combining finite element results and micromechanical methods to determine the effective reinforcing modulus of a wavy embedded nanotube. This effective reinforcing modulus (ERM) is then used within a multiphase micromechanics model to predict the effective modulus of a polymer reinforced with a distribution of wavy nanotubes. We found that even slight nanotube curvature significantly reduces the effective reinforcement when compared to straight nanotubes. These results suggest that nanotube waviness may be an additional mechanism limiting the modulus enhancement of nanotube-reinforced polymers.

KEYWORDS: (A) nanostructures, (A) PMCs, (B) mechanical properties, (B) modeling, (C) FEA

[*] Current address: Bradshaw Research Corporation, 601 W. 113st St., Suite 5C, New York, NY 10025
[**] Corresponding author. phone: +1-847-467-2347; fax: +1-847-491-3915; email: cbrinson@northwestern.edu

1. Introduction

Since their discovery in the early 1990s, carbon nanotubes have excited both scientists and engineers with their wide range of unusual physical properties. These outstanding physical properties are a direct result of the near-perfect microstructure of the nanotubes (NTs), which at the atomic scale can be thought of as a hexagonal sheet of carbon atoms rolled into a seamless, quasi-one-dimensional cylindrical shape. Besides their extremely small size, it has been suggested that carbon nanotubes are half as dense as aluminum, have tensile strengths twenty times that of high strength steel alloys, have current carrying capacities 1000 times that of copper, and transmit heat twice as well as pure diamond [1]. To take advantage of this unique combination of size and properties, a wide variety of applications have been proposed for carbon nanotubes, including chemical and genetic probes, field emission tips, mechanical memory, ultrafine sensors, hydrogen and ion storage, scanning probe microscope tips, and as structural materials [1]. It has been suggested that nanotechnology, largely fueled by the remarkable properties of carbon nanotubes, may ultimately transform technology to a greater extent than the advances of the silicon revolution [2].

In this paper we will focus on the use of carbon nanotubes as the reinforcing phase in a bulk polymer material. Preliminary experimental results suggest that small amounts of carbon nanotubes can significantly enhance the overall mechanical behavior of the polymer [3-7]; we refer to these materials as *nanotube reinforced polymers* (NRPs). Other types of nanoscale inclusions, including boron nitride (BN) nanotubes [8, 9], nanoclays, and nanowires, while not directly addressed in this paper, have also been proposed as candidate filler materials. NRPs hold vast potential as structural materials due to the extremely high strength- and modulus-to-weight

ratios that are likely to be achieved with such materials. Other potential advantages of NRPs include multifunctionality (utilizing the outstanding electrical properties of the NTs), increased energy absorbance, higher toughness, and ease of manufacturing (particularly if the NRPs can be processed using traditional polymer techniques). Despite the challenges which these materials present in terms of modeling, processing, and most notably the availability and cost of the raw nanotube material, the preliminary results and inherent potential suggest that further study of NRPs is warranted.

To increase our understanding of these materials it is useful to develop models to predict the effective properties of NRPs, enabling detailed study of the material response. One means to accomplish this is the extension of traditional micromechanics and composite models that address particular characteristics of these materials. Because micrograph images show that the embedded nanotubes remain highly curved when dispersed in a polymer (see Figure 1), we have developed a hybrid finite element-micromechanical model that allows the effects of embedded nanotube waviness to be incorporated into traditional micromechanical techniques. Using experimental data we demonstrate that nanotube waviness can limit NRP modulus enhancement, resulting in improvements that (while still significant) are currently less than predicted by traditional theories.

At the moment it is impossible to differentiate the impact of nanotube waviness from competing reinforcement-limiting mechanisms such as bonding, dispersion and NT degradation in existing NRP experimental data. Nevertheless, our results provide a clear picture of how relatively moderate waviness can hinder the effectiveness of NTs as structural reinforcement. While the work reported here is an application of a micromechanics method to a nanostructured material, the integration of atomic scale modeling could readily be adapted into such an analysis.

In the future a fusion of true nanoscale and microscale modeling will provide even more insight into this material behavior.

The following section discusses the properties of carbon nanotubes and issues related to their use in structural polymers. The micromechanical and finite element models that were used in this work, and a description of how inclusion waviness was integrated into micromechanical property predictions, will follow. We then present results showing how the effective reinforcing modulus of an embedded wavy nanotube is dependent on geometry and other parameters. Finally, the effective modulus predictions for NRPs with various nanotube orientations are predicted and compared to experimental data.

2. BACKGROUND

Due to the inherent strength of the carbon-carbon bond and the potential of a defect-free microstructure, it has been suggested that nanotubes may approach the theoretical limits for many important mechanical properties, including axial stiffness and tensile strength. Large increases in the fracture strain and toughness, and superior electrical/thermal properties, are other potential benefits of using NTs as the filler material in a polymer-based composite. One possible near-term application of carbon nanotubes, which is the motivation for this work, is as a low volume-fraction structural reinforcement in a polymer matrix.

Carbon nanotubes can be broadly classified into three categories: single-walled nanotubes (SWNT), multi-walled nanotubes (MWNT), and nanotube bundles or ropes (see Figure 2). SWNTs consist of single layer of carbon atoms wrapped into a cylindrical shape, while MWNTs consist of several concentric layers (or shells) of individual carbon nanotubes that are weakly

coupled to each other through van der Waals forces. The spacing between these individual shells is on the order of 0.34 nm, which is slightly larger than interlayer spacing in a graphene sheet. Typically, however, the nanotubes are found to have self-organized into crystalline bundles [10, 11], consisting of several to hundreds of SWNTs or MWNTs arranged in a closest-packed two-dimensional lattice. Within these bundles the nanotubes normally display a monodisperse range of diameters, with adjacent tubes weakly coupled via van der Waal interactions. While not modeled in the continuum approach presented here, explicit differences in the structural behavior of these various NT forms, particularly when embedded within a polymer, will need to be addressed in the future. While SWNTs are more susceptible to bending due to their extremely small cross-sections, more intimate contact with the polymer matrix may lead to more efficient stress transfer between the two phases. For MWNTs and NT bundles, inter-layer sliding (so-called "sword and sheath" slippage [12]) and weak inter-tube coupling, respectively, could hinder load transfer between the phases.

Much of the early work studying the mechanical properties of nanotubes utilized computational methods such as molecular dynamics and *ab initio* models. These models focused primarily on SWNTs because of the increase in computational resources necessary to model larger systems. In general these computational studies have found nominal values for the axial Young's modulus on the order of 1 TPa, with values for the Poisson ratio approximately 0.20 to 0.30 [13-16].[1] A different approach calculated elastic moduli of roughly 1 TPa for SWNTs and MWNTs, while SWNT bundle moduli ranged between 0.4 and 0.8 TPa and were dependent on the diameter of the individual tubes [19]. Most of these models assume defect-free nanotubes; nanotubes with a significant number of defects (such as those produced via catalytic methods)

[1] It should be noted that other researchers have suggested that in order to properly model the bending behavior of the nanotubes, more appropriate values for the Young's modulus and the shell thickness would be on the order of 5 TPa and 0.067 nm, respectively [17, 18]. However, the values in the main text will be used in the current work.

are expected to have much lower moduli values [20]. More recently, a great deal of progress has been realized in the manipulating and testing of individual nanotubes and nanotube bundles [20-27]; in general these experiments have validated the predicted modulus values (see Table 1).

One issue of practical importance for NRPs is the separation and dispersion of the nanotubes within the matrix, which is critical as the nanotubes tend to assemble into ropes or bundles due to van der Waals interactions between the individual tubes. While some researchers have been able to separate individual nanotubes from the bundles via ultrasound and polar solvents, maintaining separated nanotubes during the processing of NRPs is still the subject of ongoing work. Some results suggest that the use of a surfactant as a coupling agent may overcome the van der Waals attractive force and allow good dispersion of the nanotubes within a polymer [7]. However, it is unclear whether such processing agents can be employed to promote nanotubes dispersion without compromising the bonding between nanotubes and polymer.

Optimal material properties will be achievable only if the orientation of the nanotubes within the polymer can be controlled, and several techniques have been proposed to address this issue. Ajayan and co-workers [28] found that cutting thin slices (on the order of 100 nm) of a nanotube-reinforced epoxy film introduced preferential orientation via shear flow. However, this method was only successful for thin slices and may not be applicable for nanotube orientation in a bulk polymer. An alternative method that may be more suitable for larger samples is tensile loading of the NRP at temperatures greater than the glass transition temperature of the polymer [29, 30]. A combination of solvent casting and melt mixing was also found to produce a high degree of nanotube alignment [31]. While individual SWNTs and SWNT ropes have been aligned in the presence of a strong magnetic field [32], to our knowledge this method has not been extended to nanotube-reinforced polymers.

Another topic currently being studied is the NT-polymer interface and load transfer between the polymer and the nanotubes [3-5, 30, 33-36]. While poor load transfer for MWNTs and SWNT ropes embedded in a polymer has been attributed to the relative slipping of individual tubes within the MWNT and the rope, respectively [3, 34], other researchers have found evidence of promising nanotube-polymer interactions in composite materials. For example, strong bonding between MWNTs and polystyrene (PS) [5] and polyhydroxyaminoether (PHAE) [29] has been reported. Analysis of SWNT bundles-PMMA thin films found that PMMA was able to intercalate within the bundles, which would likely enhance the interface between the nanotube and polymer phases [37]; significant wetting and interfacial adhesion for SWNT bundles embedded in an epoxy resin has also been reported [38]. A recent molecular dynamics study suggested that polymer morphology, and specifically the helical wrapping of the polymer around the nanotubes, was a key factor influencing the strength of the interface [35]. Functionalization of the NT to increase its chemical reactivity has also been proposed as means to further enhance nanotube-polymer interaction [39]. While it has been estimated that the stress transfer efficiency between NTs and a polymer matrix could be an order of magnitude larger than typically measured in conventional fiber-based composites [40], a much better understanding of the factors which influence the nanotube-polymer interface is required.

The issues identified above indicate several key aspects that will influence our ability to design and model materials that fully exploit the potential of nanoscale reinforcements. One issue which has not typically been associated with the modeling of NRPs, but which seems critical based on micrograph images of these materials, is the characteristic waviness or curvature of embedded nanotubes (see Figure 1). To address this question we have developed a model that integrates the waviness of the nanotubes into micromechanical predictions of the

NRP effective modulus. Our results suggest that such waviness, while potentially beneficial for other applications (i.e. strength), can drastically reduce the effective stiffness of the NRP when compared to straight nanotube models.

3. THE MODEL

Based on the discussion of the last section, we are interested in using micromechanical techniques to study the effective elastic moduli of nanotube-reinforced polymers. The basis of the model is to determine the *effective* reinforcing modulus (ERM) of the wavy embedded nanotube; that is, a *representative* value denoted E_{ERM} that accounts for the reduction in reinforcement provided by the wavy nanotube in comparison to the reinforcement provided by a straight NT (of modulus E_{NT}).[2] Thus while the nanotube modulus E_{NT} is a material property, the effective reinforcing modulus E_{ERM} ($E_{ERM} \leq E_{NT}$) is a material parameter that is a function of the geometry of the wavy nanotube and other variables (see the Appendix). This effective modulus is then available for use in standard micromechanical models in lieu of the true (actual) nanotube modulus. While such a procedure can be applied in general to any class of curved and wavy inclusions, embedded nanotubes and NRPs are the focus of the present discussion.

In this regard, we note the results of several researchers who found that continuum models provide useful insight into nanotube behavior [42, 43], despite the discrete nature of their atomic structure.[3] To simplify the geometry we will treat the nanotube geometry as a solid

[2] This effective reinforcing modulus E_{ERM} is identical to what we have called the wavy nanotube modulus (E_{wavy}) in previous work [41].

[3] Others have found a large number of atomic layers was necessary to justify the treatment of the nanotube as a continuum [44]. However, for the purposes of moduli predictions we believe that a continuum assumption is an acceptable simplification. Other mechanical behavior, such as crack propagation and fracture, will undoubtedly be more dependent on atomic structure and may be especially ill-suited for such an assumption.

element of circular cross-sectional area, which implicitly introduces two simplifications into the analysis. First, treating the inclusion as a solid cylinder neglects the hollow nature of the nanotubes.[4] Second, by modeling the nanotube as a continuum we are disregarding the specific form of the nanotube (SWNT, MWNT, or bundle) and neglecting any possible relative motion between individual shells or tubes in a MWNT and an NT bundle, respectively. Each of these assumptions suggests that E_{ERM} as calculated here is an "upper bound" for the given model, in that accounting for the hollow nature of the NTs or modeling sliding of the tubes or shells would further reduce the effective stiffness of a wavy nanotube. Thus nanotube waviness may be even more significant than the results presented in this work would indicate. While this approach will highlight the impact of nanotube waviness on the effective modulus of an NRP, a more rigorous analysis that accounts for the discrete nature of the nanotube and the atomic interaction between the nanotube and polymer is warranted and will be the subject of future work.

In addition to the continuum assumption, several other simplifications are invoked throughout this work to aid in the interpretation of the results. The individual phase materials are modeled as linear elastic and isotropic, and perfect bonding between the phases is assumed. The waviness of a nanotube of diameter *d* will be introduced by prescribing an embedded NT shape of the form $y = a\cos(2\pi z/\lambda)$, where λ is the sinusoidal wavelength and *z* is the fiber axial direction (see Figure 3). Unless otherwise noted, Poisson ratios of 0.30 were assumed for all phases in the simulations; this value is representative of a wide range of polymer materials, and is consistent with the range of values estimated for carbon nanotubes. This assumption will be discussed in more detail later in this paper.

[4] It is also well established that in many cases the cross-section of the nanotubes is not circular but is typically distorted due to van der Waals interactions between the shells (or tubes). However, for our current investigation the effect of this slight distortion in cross-sectional shape is negligible.

The details of the finite element analysis of an embedded wavy nanotube, which considers the constraint of the surrounding matrix, follows. Next, the formulation of the Mori-Tanaka method for a multiphase composite with randomly aligned cylindrical inclusions in two- and three-dimensional space will be presented. Finally, a multiphase composite analysis where the nanotubes are modeled as a finite number of discrete inclusion phases with different effective moduli based on their embedded waviness, is discussed.

3.1 FINITE ELEMENT ANALYSIS

To determine the effective reinforcing moduli E_{ERM} of an embedded wavy nanotube, ANSYS^{TM} was used to create and analyze a three dimensional finite element model of a single, infinitely long wavy nanotube of diameter *d* perfectly bonded within a matrix material. For axial loading the problem is symmetric about the $x=0$ and $z=n\lambda/2$ (where *n* is an integer) planes; thus the quarter-symmetric unit cell shown in Figure 3 is used for the analysis. The size of the cell was chosen such that the effective cell response is independent of additional matrix material (see the Appendix). A more complete discussion of the finite element modeling used here is provided in the second part of this paper [45].

For the finite element simulations symmetry conditions $u_x=0$ and $u_z=0$ were prescribed on the $x=0$ and $z=0$ planes, respectively. The model was constrained in the *y* direction at a single point to prevent free body translation, and an infinitesimally small axial displacement, Δ, prescribed to all nodes on the plane $z=\lambda/2$. The effective modulus of the cell is defined as

$$E_{cell}^{FEA} = \frac{F_{tot}\,\lambda}{2A\Delta}, \qquad (1)$$

where F_{tot} is the sum of all nodal resultant forces on the displaced plane and A is the cross-sectional area of the cell.

In order to extract the effective reinforcing moduli of the *embedded* wavy inclusion (as it exists in the matrix) from (1), we propose a parallel model of the effective cell response, independent of the previous analysis,

$$E_{cell}^{parallel} = c_{NT} E_{ERM} + (1 - c_{NT}) E_{matrix}, \tag{2}$$

where c_{NT} is the nanotube volume fraction within the finite element cell and E_{matrix} is the matrix modulus. From (1) and (2), E_{ERM} of the embedded inclusion can be calculated as

$$E_{ERM} = \frac{E_{cell}^{FEA} - (1 - c_{NT}) E_{matrix}}{c_{NT}}. \tag{3}$$

Thus E_{ERM} represents the modulus of a straight inclusion that, under identical loading conditions, would yield the same effective cell response as that obtained with the wavy inclusion.

This finite element solution is a powerful tool to model the effective response of embedded wavy inclusions. While at first glance the number of parameters affecting E_{ERM} appears quite large, in the appendix we show that for the model described above, and the assumption that the Poisson ratios of the phases are equal, E_{ERM} will only be dependent on three variables: the waviness ratio ($w=a/\lambda$) and wavelength ratio (λ/d) of the nanotube and the ratio of the phase moduli ($E_{ratio} = E_{NT}/E_{matrix}$). A systematic analysis of the impact of these parameters on

E_{ERM} was undertaken and the key results will be presented in Section 4 of this paper. The benefit of such an analysis is that it allows inclusion waviness to be integrated into traditional micromechanics techniques by simply modeling the wavy inclusions as straight inclusions with a reduced reinforcing modulus E_{ERM} based on the embedded geometry and determined via finite element modeling.

3.2 MICROMECHANICAL ANALYSIS

We will illustrate how inclusion waviness can be incorporated into traditional micromechanical techniques by using the Mori-Tanaka method, a popular tool for the analysis of multi-phase materials [46-48]. The Mori-Tanaka method has been used by a wide range of researchers to model the effective behavior of composites, and allows the average stress fields and overall effective stiffness of a composite with a non-dilute concentration of inclusions to be determined. It has been used to study the effect of inclusion shape on composite moduli [49, 50] and the viscoelastic behavior of polymer-matrix composites [51, 52]. Furthermore, the Mori-Tanaka method has been extended to cover composites with multiple inclusion phases [47, 48] and random orientations of inclusions [53].

For completeness we briefly outline the derivation of the Mori-Tanaka method below (see [48] for a more complete derivation). We assume that the composite is comprised of N phases; the matrix will be denoted as phase 0 with a corresponding stiffness C_0 and volume fraction f_0, while an arbitrary rth inclusion phase (where r=1 to N-1) has a stiffness of C_r and a volume fraction f_r. For simplicity we will assume that all fiber phases can be modeled as infinitely long cylindrical inclusions.

Now consider the response of the composite to a uniform far-field applied strain ε_a on the boundary. The average strain field within the matrix will not be uniform, due to the presence of the inclusions, but rather will be perturbed by an amount $\left\langle \varepsilon_0^{pt} \right\rangle$, such that

$$\left\langle \varepsilon_0 \right\rangle = \varepsilon_a + \left\langle \varepsilon_0^{pt} \right\rangle, \tag{4}$$

where the symbol $\langle\ \rangle$ denotes a volume averaged quantity. The average strain in the *r*th inclusion is further perturbed from that of the matrix,

$$\left\langle \varepsilon_r \right\rangle = \left\langle \varepsilon_0 \right\rangle + \varepsilon_r^{pt}. \tag{5}$$

Using the equivalent inclusion method, the average stress in the *r*th inclusion can be written in terms of the matrix stiffness,

$$C_r \left\langle \varepsilon_r \right\rangle = C_0 \left(\left\langle \varepsilon_r \right\rangle - \varepsilon_r^* \right), \tag{6}$$

where ε_r^* is the ficticious eigenstrain of the *r*th inclusion. For ellipsoidal inclusions, Eshelby showed that the eigenstrain and perturbed strain of the *r*th inclusion are related via

$$\varepsilon_r^{pt} = S_r \varepsilon_r^*, \tag{7}$$

where S_r is the Eshelby tensor, given in Appendix 3 for an infinitely long cylindrical inclusions aligned along the x_3 axis.

Solving for ε_r^* in (6) and then substituting into (5) using (7), one can find the dilute strain-concentration factor of the *r*th phase, A_r^{dil}, such that

$$\langle \varepsilon_r \rangle = A_r^{dil} \langle \varepsilon_0 \rangle, \tag{8}$$

where

$$A_r^{dil} = \left[\mathbf{I} + S_r C_0^{-1} (C_r - C_0) \right]^{-1}, \tag{9}$$

and **I** is the fourth order identity tensor. Given (8), the effective composite stiffness *C* is defined as the relationship between the sum of the volume-weighted stresses and volume-weighted strains of each phase, such that

$$C = \left(\sum_{r=0}^{N-1} f_r \left\{ C_r A_r^{dil} \right\} \right) \left(\sum_{r=0}^{N-1} f_r \left\{ A_r^{dil} \right\} \right)^{-1} \tag{10}$$

where the curly brackets $\{\ \}$ represent an orientational average[5] (necessary to account for random orientations of inclusions) and $A_0^{dil} = \mathbf{I}$ by definition. Once the components of the

[5] The orientational average of a fourth-order tensor is $\left\{ B_{ijkl} \right\} = \frac{1}{\alpha} \int_{\Omega} a_{ir} a_{js} a_{kt} a_{lu} B_{rstu} \, d\Omega$, where Ω represents the orientational space, a_{ij} are the components of the appropriate transformation matrix relating local to global coordinates, B_{rstu} is the fourth-order tensor in the local coordinate system, and α is an integration factor. Explicit expressions for the orientational averages for 2D and 3D random orientations are given elsewhere [54]. For unidirectional inclusions orientational averaging is not required and the brackets in (10) can be dropped.

effective stiffness have been determined, the standard relationships can be used to find the corresponding elastic constants.

To model the nanotube-reinforced polymer we partition the nanotube inclusions into distinct phases, based on their embedded waviness, and treat the problem as that of a multiphase composite. Each nanotube phase is assigned a distinct effective reinforcing modulus E_{ERM}, based on the average waviness of the phase and the results of the preceding finite element analysis. In practice, such a solution could be developed by imaging a representative portion of the NRP and developing an appropriate waviness distribution function characterizing the magnitude and pervasiveness of the nanotube waviness, leading to an appropriate multiphase composite model (see Figures 4 and 5). This waviness distribution, along with the spatial orientation of the NTs, can be used within an appropriate micromechanical method to provide a refined estimate of the effective moduli of a nanotube-reinforced polymer. This is demonstrated in the next section using the Mori-Tanaka method for 2D and 3D randomly orientated inclusions [see equation (10)] for an assumed distribution of nanotube waviness.

The critical step of the analysis is the determination of the dilute strain-concentration tensor A_r^{dil} relating the average strain of the *r*th inclusion to that of the matrix. In the present analysis A_r^{dil} is found via (9) where the stiffness tensor(s) of the inclusion phase(s) C_r are found using the appropriate values of E_{ERM} (based on the previous section and assuming that the Poisson ratio of the inclusion remains unchanged), and where the Eshelby tensors S_r are for cylindrical inclusions. Thus to account for the waviness of a particular inclusion we first find E_{ERM}, based on the embedded geometry and other applicable parameters, via a finite element analysis. We then treat the wavy inclusion as a straight inclusion but with an adjusted stiffness tensor to account for the wavy geometry. In a related work we show that A_r^{dil} can be computed

directly from an appropriate finite element analysis [45]; in either case once A_r^{dil} has been determined the implementation of the Mori-Tanaka solution remains unchanged.

Our results suggest that modeling the NTs as straight inclusions (i.e. neglecting the curvature of the embedded geometry) is a simplification that will severely overestimate the reinforcement that the NTs provide the polymer. While the procedure here is demonstrated using E_{ERM} calculations based on finite element results, alternative means to evaluate E_{ERM}, such as molecular dynamics or an extension of the equivalent continuum model [55], could also be used in a similar analysis. Adaptations of the current model to include such effects as inter-layer (MWNTs) and inter-tube (NT bundles) sliding, as well as imperfect bonding between the nanotubes and the polymer, while not addressed here could also be developed.

4. RESULTS

The objective of this work is to develop a method to incorporate the typically observed waviness of embedded nanotubes into standard micromechanics techniques. Because the nanotube has been modeled as a continuum, the method is also in general applicable to other types of inclusions that may exhibit similar embedded geometries. We note that E_{ERM} will be less than (or equal to) the true NT modulus due to its waviness, and that a distribution of NT waviness within the material is likely. Thus rather than treat the NRP as two-phase (nanotube/polymer) composite, we have developed a multiphase composite model where the NTs are partitioned into distinct phases and assigned characteristic E_{ERM} based on their embedded waviness.

Before we begin our analysis it is insightful to estimate the range of values that may be characteristic of the waviness and wavelength ratios associated with the wavy geometry of embedded nanotubes. For illustrative purposes, Figure 4 shows an image of an NRP with different wavy nanotubes marked by solid lines, with approximate values for a/λ and λ/d given in the inset. We will show in this section that for even relatively minor waviness, the decrease in effective reinforcement can be appreciable.

Several nanotubes in Figure 4 are approximately straight (and not identified in the inset), while others show kinks and bends which, while not demonstrating the exact sinusoidal shape assumed in the model, will similarly limit the effective reinforcement of those nanotubes. Finally we note that waviness perpendicular to the plane of the picture is masked in this TEM image, and that it is possible that straightening of the NTs may have been induced during processing of the sample used in the TEM analysis. Thus the waviness parameters shown in Figure 4 are to be seen as *illustrative* only, and for a particular NRP sample will be dependent on the quality of the nanotubes and the NRP processing conditions. While a more thorough procedure to determine the NT waviness for a particular sample may be warranted, for the purposes of this paper a hypothetical waviness distribution is sufficient to show the effect of nanotube waviness on the effective modulus of an NRP.

With this in mind, the remainder of this section is divided into two parts. In the first part we discuss impact of nanotube waviness and other model parameters on E_{ERM}. We will then use these results to compare the predictions of our micromechanical analysis, accounting for the embedded nanotube geometry, with predictions obtained assuming straight nanotube inclusions and with published experimental data for NRP effective modulus.

4.1 Effective Reinforcing Modulus E_{ERM}

As discussed previously (and shown in the Appendix) we have shown that the model described here can be considered to be dependent on three variables: the waviness ($w=a/\lambda$) and wavelength ratio (λ/d) of the nanotube and the ratio of the phase moduli (E_{ratio}). Figure 6 shows E_{ERM} as a function of waviness for several different values of E_{ratio} and a wavelength ratio of 100. For all simulations a matrix modulus of 1 GPa was used. As expected for zero waviness we obtain the straight nanotube results $E_{ERM} = E_{NT}$. In addition we see that E_{ERM} is strongly dependent on the waviness and quickly decreases with increasing nanotube curvature. This behavior is less pronounced for smaller E_{ratio} values because of the mechanical constraint that the surrounding matrix material provides the embedded wavy nanotube.

Figure 7 shows the dependence of E_{ERM} on the wavelength ratio of the nanotube for different values of waviness and E_{ratio}=200. We see that for increasingly large wavelength ratios the value of E_{ERM} converges to a constant value (dependent on the waviness). Note that the critical wavelength ratio at which E_{ERM} can be considered to have reached a maximum is dependent on the waviness such that for a given value of waviness nanotubes with larger wavelength ratio act stiffer. While we have shown that for longer wavelength ratios ($\lambda/d > 1000$) curves of E_{ERM} versus waviness for different values of E_{ratio} can be superposed via vertical shifting [54], for practical NRP materials the wavelength ratio is much smaller. Unless otherwise specified, to simplify the remainder of this section we will only consider wavelength ratios of 100.

In Figure 8 E_{ERM} (normalized with respect to E_{NT}) is presented as a function of E_{ratio} for different values of waviness with $\lambda/d = 100$. Note that when the phase moduli are equal ($E_{ratio} =$

1) the finite element cell is homogeneous such that $E_{ERM}=E_{NT}=E_{matrix}$ as shown; while not shown explicitly in the Figure all curves monotonically approach this point. With this in mind we note the strong initial decrease in E_{ERM}/E_{NT} for small values of E_{ratio}, revealing the critical role of the mechanical constraint of surrounding matrix for this case. As E_{ratio} increases the impact of the mechanical constraint diminishes, resulting in minimal changes in E_{ERM}/E_{NT} for larger values of E_{ratio} (in the limit as $E_{ratio} \rightarrow \infty$ the response is that of a free-standing wavy rod). From Figure 8 the impact of nanotube waviness on E_{ERM} is again evident; for w=0.056 the effective reinforcement provided by the wavy nanotube decreases by almost 20% for an E_{ratio} of 200, a modulus ratio representative of those anticipated for NRPs. For larger values of waviness the decrease in E_{ERM} is even more apparent. Note that in our simulations we are interested in the *initial* reinforcing modulus of the wavy nanotube, and do not consider the effects of nanotube straightening due to the application of an applied load.

For all previous simulations the Poisson ratios of the matrix and nanotube were assumed to be equal ($\nu_{NT}=\nu_{mat}=0.30$) to simplify the analysis. For many practical nanotube-polymer systems the difference in Poisson ratio is expected to be relatively small, with ν_{NT} typically predicted in the range of 0.20-0.30 and ν_{mat} for a typical structural polymer approximately 0.25-0.40. To check the validity of this assumption simulations were conducted where the wavy NT parameters were held constant (E_{ratio} = 200, λ/d = 1000, and w = 0.1) while varying the Poisson ratio of each phase (see Figure 9). We found that the effect of the Poisson ratio of the nanotube on the simulation is negligible, which is not surprising considering the small volume fraction of nanotube (< 0.05%) modeled in the cell to provide the dilute approximation. While the effect of ν_{mat} is more apparent, we note that for these results the difference in E_{ERM} is only approximately

5% for ν_{mat} between 0.25 and 0.40. Thus the results presented in this paper for common Poisson ratios are in general applicable to a wide range of typical NT-polymer composite materials.

In summary, we have found that the effective reinforcing modulus (E_{ERM}) of an embedded, wavy nanotube is strongly dependent on its geometry and the ratio of the phase moduli. As expected, the stiffening effect of the wavy nanotube decreases as the waviness of the nanotube increases, while stiffening increases as the wavelength ratio of the wavy nanotube λ/d increases. We have also shown that E_{ERM} is a function of the ratio of the phase moduli, as the constraint of the surrounding matrix on the straightening of the wavy nanotube can be significant. Further, we have seen that for values of these parameters which are likely to be representative of the wavy nanotubes embedded in a polymer matrix, this reduction in effective modulus can be quite substantial, suggesting that the waviness of the embedded nanotubes will result in less than optimal reinforcement. In the following section we will illustrate the impact of this waviness on the effective moduli of an NRP nanotube via a micromechanical analysis.

4.2 Micromechanical Effective Modulus Predictions using E_{ERM}

In the previous section we have seen how the effective reinforcing modulus of an embedded wavy nanotube is dependent on the geometry of the NT and other parameters. The results of the previous section can now be used within traditional micromechanics techniques for predictions of the effective modulus of NRPs. Here we highlight this procedure (see Figure 5) by comparing effective modulus predictions obtained using the Mori-Tanaka method with experimental tensile modulus data for various loadings of MWNTs in polysytrene (Dow 666) [6]. The nanotubes used in this study were catalytically grown via a chemical vapor deposition

process using Xylene-ferrocene [56] and dispersed within the polystyrene matrix via shear mixing in a Haake Polylab bowl mixer. While the researchers report good dispersion of the NTs within the matrix, in situ TEM straining studies have found evidence of inadequate bonding between the phases [57].

Figures 10 and 11 presents the experimental data for the effective tensile modulus as a function of volume fraction of MWNTs, together with the Mori-Tanaka predictions assuming a single phase of *straight* NT inclusions, for randomly orientated inclusions in 3D and 2D space, respectively. Also shown are the predictions obtained considering nanotube waviness by assuming each of the nanotube waviness distributions given in Table 2. Lacking an appropriate image of the nanostructure of the material, these waviness distributions are loosely based on the NRP images shown in Figure 1 and represent two potential types of waviness (minimal waviness and more moderate waviness) that may be anticipated for nanotubes embedded in a polymer matrix.[6] For each waviness distribution the effective reinforcing moduli for each nanotube phase was estimated using E_{ERM} from the preceding finite element analysis for E_{ratio}=200 (with λ/d = 100); these values were then scaled for an NT modulus of 450 GPa[58] and are given in Table 2. Given the waviness distribution and the appropriate values of E_{ERM} the multiphase composite analysis described in the previous section can be implemented.

What is most striking about the results presented in Figures 10 and 11 is the large discrepancy between the Mori-Tanaka predictions assuming *straight* nanotubes and the experimentally measured moduli. While the experimental modulus has been enhanced significantly with the addition of the NTs (the modulus increases by a factor of two for 15 vol% NT), the realized improvements in modulus are significantly less than the micromechanics

[6] While it would be desirable to image a representative portion of the NRP to obtain the waviness distribution, our results clearly demonstrate how nanotube waviness can significantly decrease the predicted effective properties of the material.

predictions assuming straight nanotubes. Integrating moderate nanotube waviness (NT distribution w2) into the effective moduli predictions is shown to drastically decrease the moduli predictions, suggesting that NT waviness may be one factor limiting the modulus enhancement of NRPs.

Similar results are found using other NRP experimental data found in the literature. Figure 12 shows the experimental modulus and micromechanics predictions obtained for 5 wt% MWNTs embedded in epoxy [3], using the second waviness distribution (see Table 2) with corresponding E_{ERM} values found in the same manner as outlined earlier. Again the results show that the micromechanics predictions for randomly orientated *wavy* NTs, assuming moderate NT waviness, can reduce the predicted effective modulus of the NRP by a factor of two or more in comparison to the predictions obtained assuming straight NTs. A reduction in effective modulus is also evident when comparing the micromechanical predictions for a unidirectionally aligned NRP with wavy versus straight nanotubes.

In the existing experimental data it is impossible to distinguish the effects of nanotube waviness from other mechanisms that would tend to decrease the effective properties of the nanotube-reinforced polymer. Other conditions, such as poor bonding, inadequate dispersion, and nanotube degradation, can also reduce the experimental moduli of the NRPs. However, based on images of nanotubes embedded in polymer films and the results presented in this paper, we have demonstrated that nanotube waviness is an additional mechanism which can strongly control the effectiveness of nanotubes as structural reinforcement.

CONCLUSIONS

Motivated by micrographs showing that nanotubes embedded within polymers often exhibit significant curvature, we have developed a model that incorporates this curvature into traditional micromechanical methods via a multiphase composite approach. Finite element results of embedded wavy inclusions show that the effective reinforcing moduli of the inclusions quickly decreases as a function of the inclusion waviness and is also dependent on the wavelength ratio and the ratio of the phase moduli. Using material properties representative of nanotube-reinforced composites, we have shown that nanotube waviness can reduce the predicted effective moduli of these materials by a factor of two or more, and may be one reason why the modulus enhancement of NRPs, while significant, is somewhat less than predicted using standard micromechanical techniques. While for some applications (such as impact resistance and energy absorption) nanotube waviness may be beneficial, for structural applications inclusion waviness can significantly affect the magnitude of modulus enhancement which the nanotubes provide the host polymer material.

While the procedure here is demonstrated using E_{ERM} calculations based on finite element results, alternative means to determine the appropriate value of E_{ERM}, incorporating more detailed information on the atomic level interactions in the material, could also be used in a similar analysis. Adaptations of the current model to include inter-layer (MWNTs) and inter-tube (NT bundles) sliding, as well as imperfect bonding between the nanotubes and the polymer, were not addressed here and warrant further work. While at the moment it is impossible to isolate the effects of nanotube waviness from other reinforcement-limiting mechanisms, such as poor bonding and dispersion, these results demonstrate that nanotube waviness can severely limit the effective modulus of nanotube-reinforced polymers.

Finally, our results suggest that methods of NRP fabrication that reduce the waviness of embedded NTs would allow the NTs to provide maximum structural reinforcement. From our results one can also hypothesize that nanotube waviness may be one reason why NRP modulus enhancement has sometimes only been reported at higher temperatures [4, 59]; if compressive stresses developed during the polymer cure introduce bending (and hence curvature) into the nanotubes, significant NT reinforcement may only be realized as the NTs straighten due to polymer softening at elevated temperatures.

ACKNOWLEDGMENTS

This work was supported by the NASA Langley Computational Materials Nanotechnology Program. We would like to thank Dr. Rodney Andrews of the University of Kentucky for advanced access to his experimental data and Dr. Linda Schadler of RPI for fruitful discussions.

Appendix

APPENDIX 1. CONVERGENCE OF E_{ERM} FOR A SUFFICIENTLY LARGE MATRIX

In order to eliminate the size of the finite element model as a parameter in the analysis, it is necessary to show that E_{ERM} converges for a sufficiently large matrix. To accomplish this we consider a finite element cell of an embedded wavy nanotube (see Figure 3), where for simplicity we redefine the length of the cell as L (to eliminate carrying a factor of two in our analysis below). We assume that the matrix boundary at the top and bottom of the cells is sufficiently far from the nanotube such that fields at these boundaries are undisturbed by the presence of the nanotube, and denote the volumes of the NT, matrix, and total cell as V_{NT}, V_{mat}, and V, respectively. Note that a respective area is given as A=V/L. In our model we apply an infinitesimally small uniform strain ε_z in the fiber axial direction and measure the total resultant force F_{tot} necessary to cause this strain. From (1) and (3) we can write the effective NT modulus for this particular finite element cell as

$$E_{ERM_1} = \frac{\frac{F_{tot}\,L}{V\,\varepsilon_z} - \frac{V_{mat}}{V}E_{mat}}{\frac{V_{NT}}{V}} = \frac{F_{tot}\,L}{V_{NT}\,\varepsilon_z} - \frac{V_{mat}}{V_{NT}}E_{mat}\,. \qquad (1)$$

Now consider a second finite element geometry, identical to the previous cell except that additional matrix material, with a volume V_{mat2}, has been evenly divided between the top and bottom of the first cell. Due to the size of the first cell this additional matrix material is also unaffected by the presence of the wavy nanotube, thus the force necessary to produce a uniform

strain ε_z in this additional material is $F_2 = \frac{E_{mat} V_{mat_2} \varepsilon_z}{L}$. The effective modulus calculated from the second finite element cell is then

$$E_{ERM_2} = \frac{\frac{(F_{tot} + F_2)L}{(V + V_{mat_2})\varepsilon_z} - \frac{V_{mat} + V_{mat_2}}{V + V_{mat_2}} E_{mat}}{\frac{V_{NT}}{V + V_{mat_2}}} = \frac{(F_{tot} + F_2)L}{V_{NT}\,\varepsilon_z} - \frac{V_{mat} + V_{mat_2}}{V_{NT}} E_{mat}. \qquad (2)$$

Upon substitution of the expression for F_2 into (2) one finds that $E_{ERM1}=E_{ERM2}$, and thus for a sufficiently large matrix the value of E_{ERM} is independent of the size of the finite element cell. For all simulations the finite element cell was created large enough such that this condition was satisfied.

APPENDIX 2: REDUCTION OF E_{ERM} PARAMETERS FOR THE FINITE ELEMENT ANALYSIS

Because we have shown that E_{ERM} converges given a sufficiently large cell, it is sufficient to consider the model parameters that influence E_{cell} in the present analysis. Assuming isotropic behavior of the phase materials, the model at first appears to the dependent on seven parameters: the phase moduli (E_{NT} and E_{mat}) and Poisson ratios (ν_{NT} and ν_{mat}) of the phase materials, the diameter of the NT (d), and the amplitude (a) and wavelength (λ) describing NT waviness such that

$$E_{cell} = f(E_{NT}, E_{mat}, \nu_{NT}, \nu_{mat}, a, d, \lambda). \qquad (3)$$

To first simplify the analysis we assume that the Poisson ratios of the phases are identical and equal to 0.30, an assumption that is discussed in more detail in the text. Thus one can write (3) in a mathematically equivalent form as

$$g\left(E_{cell},E_{NT},E_{mat},a,d,\lambda\right)=0, \tag{4}$$

where *g* is dependent on these six parameters but of an unknown functional form. Using the Buckingham Pi theorem [60], we can further rewrite (4) as

$$\prod_1 = G_1\left(\prod_2,\prod_3,\ldots,\prod_{n-m}\right), \tag{5}$$

where $\prod_i$ are appropriate dimensionless ratios, *n* is the number of system variables, and *m* is the minimum number of primary dimensions. Following the standard procedure for dimensional analysis, one can write

$$\begin{aligned} \prod_1 &= E_{NT}^{a}\,\lambda^{b}\,E_{cell}, & \prod_2 &= E_{NT}^{-c}\,\lambda^{d}\,E_{mat} \\ \prod_3 &= E_{NT}^{e}\,\lambda^{f}\,a, & \prod_4 &= E_{NT}^{g}\,\lambda^{-h}\,d \end{aligned}, \tag{6}$$

where the unknown superscript parameters *a*-*h* in (6) can be determined, after which substitution into (5) yields

$$\frac{E_{cell}}{E_{NT}} = G_1\left(\frac{E_{NT}}{E_{mat}},\frac{a}{\lambda},\frac{\lambda}{d}\right), \tag{7}$$

where the form of G_1 as a function of these parameters will be determined through our finite element study.

APPENDIX 3. COMPONENTS OF THE ESHELBY S_{IJKL} TENSOR ALONG THE X_3 AXIS

Below are the components of the Eshelby tensor for a circular, cylindrical inclusion with an infinite length-to-diameter ratio ($l/d \to \infty$) parallel to the 3-axis, where ν_0 is the Poisson ratio of the matrix, and all other components of the Eshelby tensor are zero.

$$
\begin{aligned}
S_{3333} &= S_{3311} = S_{3322} = 0 \\
S_{1111} &= S_{2222} = \frac{5 - 4\nu_0}{8(1-\nu_0)} \\
S_{1122} &= S_{2211} = \frac{4\nu_0 - 1}{8(1-\nu_0)} \\
S_{1133} &= S_{2233} = \frac{\nu_0}{2(1-\nu_0)} \\
S_{1212} &= \frac{3 - 4\nu_0}{8(1-\nu_0)} \\
S_{3131} &= S_{3232} = \frac{1}{4}
\end{aligned}
\tag{8}
$$

For the general form of the Eshelby tensor valid for ellipsoidal inclusions, see [61].

Tables

Type of CNT	Method	Modulus Values	Comments
11 CNTs (diameters 6- 25 nm) [21]	Amplitude of thermal vibration within a TEM	average of 1.8 TPa; min/max of 0.40/4.15 TPa	Order of magnitude range of values
27 laser ablation SWNTs (diameters 1.0-1.5 nm) [22]	Amplitude of thermal vibration within a TEM	1.3 -0.4/+0.6 TPa	Weighted average value of 1.25 TPa
Laser ablation SWNT bundles [23]	Nanostressing stage within a SEM	320 to 1470 GPa, mean of 1002 GPa	Model of load carried by the SWNTs on rope perimeter
Carbon arc SWNT bundles (bundle diameters 3-20 nm) [24]	Beam-bending via AFM	~ 1 TPa for 3 nm diameter, decreasing to < 0.1 GPa for larger diameter	Estimated shear moduli of SWNT bundle on the order of 1 GPa
6 Carbon arc MWNTs (diameter 26-76 nm) [25]	AFM-induced lateral deflection on low friction surface	Average value of 1.28 +/- 0.59 TPa with no diameter-dependence	Modulus values for silicon carbide nanorods of ~ 600 GPa
Carbon arc MWNTs [26]	electromechanical deflection and resonance within a TEM	~ 1 TPa for small diameter (<10 nm) to 0.1 TPa for large diameter (>30 nm)	Modulus a strong function of diameter
Carbon arc MWNTs [27]	Nanostressing stage within a SEM	Modulus of outer shell from ~270 to ~950 GPa	Failure via "sword-in-sheath" mechanism
Catalytic and carbon arc MWNTs [20]	Beam-bending via AFM	Catalytic: ~ 10-50 GPa Arc: 810 –160/+410 GPa	order of magnitude increase after annealing catalytic NTs at 2500°C

Table 1. Experimental values for the Young's modulus of carbon nanotubes.

waviness (w=a/λ)	E_{ERM} (GPa)	Volume fraction	
		NT distribution 1	NT distribution 2
0	450	0.4	0.05
0.05	383	0.4	0.15
0.1	260	0.2	0.3
0.25	57	0	0.3
0.5	10	0	0.2

Table 2. Effective reinforcing moduli and hypothetical NT waviness distributions used in the wavy micromechanics calculations. E_{ERM} values are for E_{ratio}=200 and λ/d=100.

FIGURE CAPTIONS

Figure 1. Images of nanotube-reinforced polymers showing that the embedded nanotubes exhibit significant curvature within the polymer. (a) TEM image of MWNTs (1 wt%) in polystyrene. The arrows and inset in the image are from the original source and show defects in the as-prepared sample and the homogeneity of the MWNT distribution over different length scales. [5] (b) SEM image of MWNTs (50 wt%) in poly(vinyl alcohol). [4]

Figure 2. Schematic illustration of the cross-sections of different forms of nanotubes. The apparent wall thickness and intertube spacing are slightly larger than the interlayer spacing of graphene (~0.34 nm). (a) Single-walled nanotube. (b) Multi-walled nanotube. (c) Single-walled nanotube bundle (or rope), closest-packed in a 2D triangular lattice.

Figure 3. Schematic of the finite element cell model of an embedded wavy nanotube. For the particular model shown $w=a/\lambda=0.1$ and $\lambda/d=35$.

Figure 4. Illustrative example of evaluating nanotube waviness (image from [5]). (inset) Approximate values for the parameters $w=a/\lambda$ and λ/d for the highlighted nanotubes.

Figure 5. Model of an NRP using a multiphase composite analysis with a known waviness distribution function.

Figure 6. E_{ERM} as a function of nanotube waviness ratio (a/λ) for different ratios of phase moduli (for wavelength ratio $\lambda/d = 100$).

Figure 7. E_{ERM} as a function of nanotube wavelength ratio (λ/d) for different values of nanotube waviness (for $E_{ratio} = 200$).

Figure 8. Normalized E_{ERM} (with respect to E_{NT}) as a function of the ratio of the phase moduli (for $\lambda/d = 100$). For $E_{ratio} = 1$, the material is homogeneous and $E_{ERM} = 1$ as marked; all curves monotonically approach this point (not shown for clarity).

Figure 9. Effect of Poisson ratio on the E_{ERM} values calculated from the FEM simulations. ($\lambda/d = 1000$, $E_{ratio} = 200$, $w = 0.1$)

Figure 10. Experimental data (10 wt% MWNTs in polysytrene)[6] and micromechanical predictions of NRP effective moduli assuming a 3D random orientation of straight and wavy nanotubes.

Figure 11. Experimental data (10 wt% MWNTs in polysytrene)[6] and micromechanical predictions of NRP effective moduli assuming a 2D random orientation of straight and wavy nanotubes.

Figure 12. Experimental data (5 wt% MWNTs in epoxy) [3] and micromechanical predictions of NRP effective moduli assuming straight (s) and wavy (w) nanotubes with different NT orientations.

FIGURES

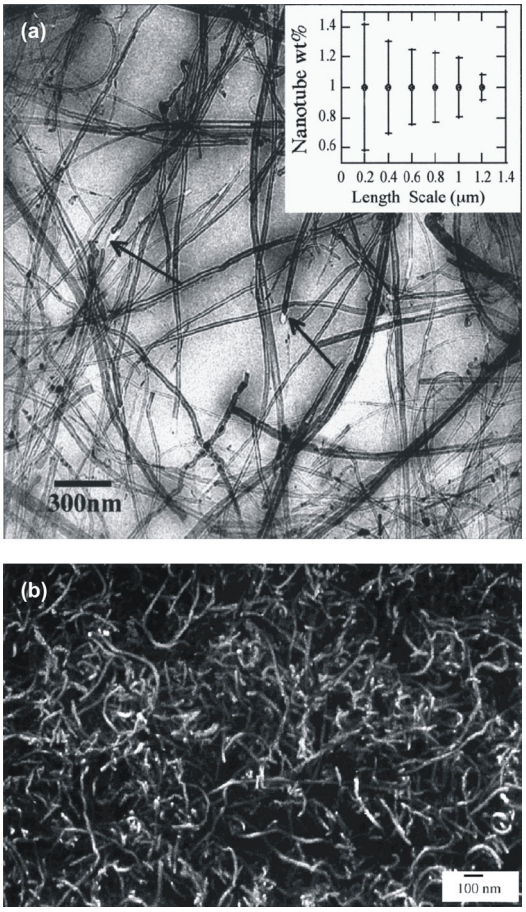

Figure 1. F. T. Fisher, R. D. Bradshaw, L. C. Brinson, "Fiber waviness in nanotube-reinforced polymer composites: I. Modulus predictions using effective nanotube properties," *Composites Science and Technology*

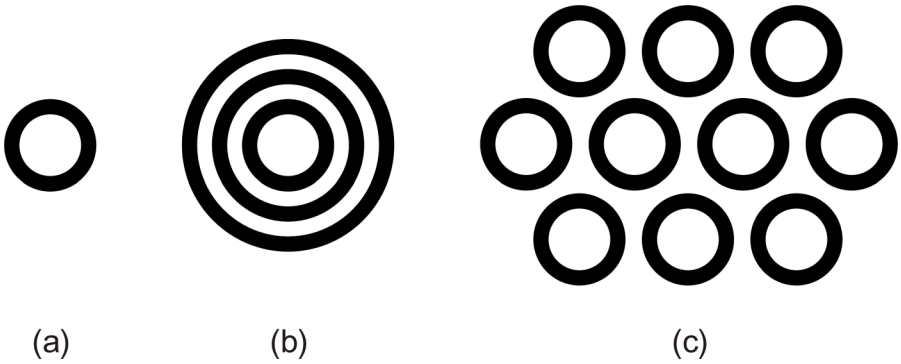

Figure 2. F. T. Fisher, R. D. Bradshaw, L. C. Brinson, "Fiber waviness in nanotube-reinforced polymer composites: I. Modulus predictions using effective nanotube properties," *Composites Science and Technology*

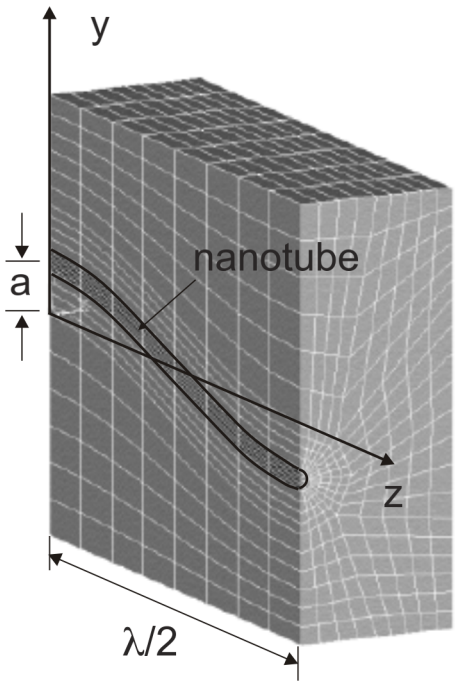

Figure 3. F. T. Fisher, R. D. Bradshaw, L. C. Brinson, "Fiber waviness in nanotube-reinforced polymer composites: I. Modulus predictions using effective nanotube properties," *Composites Science and Technology*

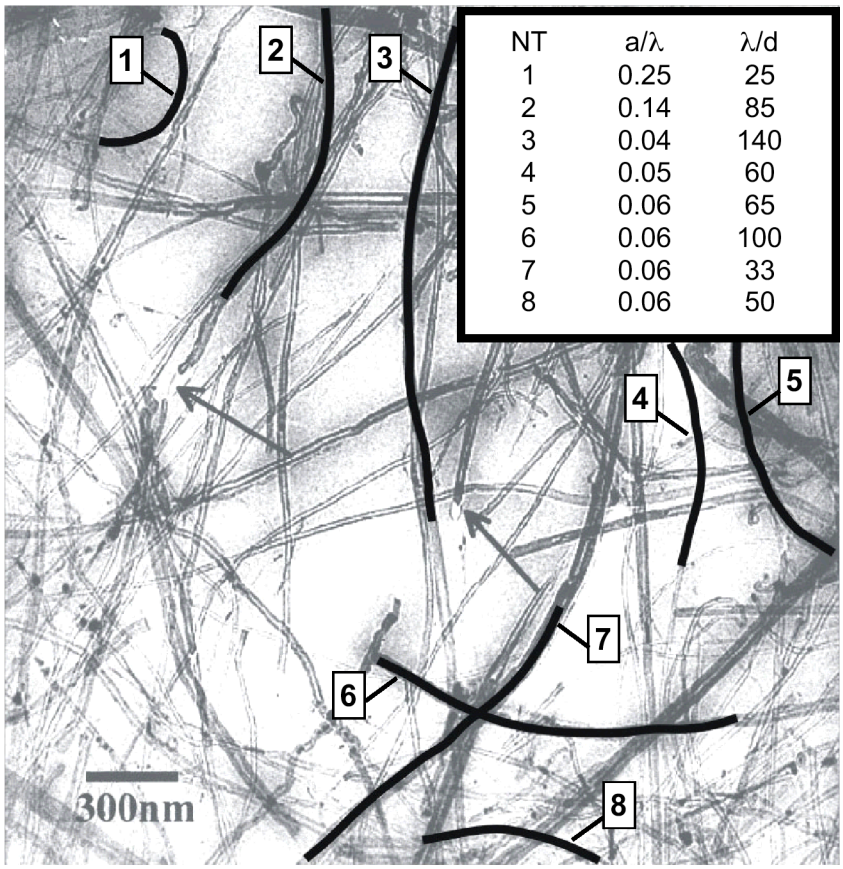

Figure 4. F. T. Fisher, R. D. Bradshaw, L. C. Brinson, "Fiber waviness in nanotube-reinforced polymer composites: I. Modulus predictions using effective nanotube properties," *Composites Science and Technology*

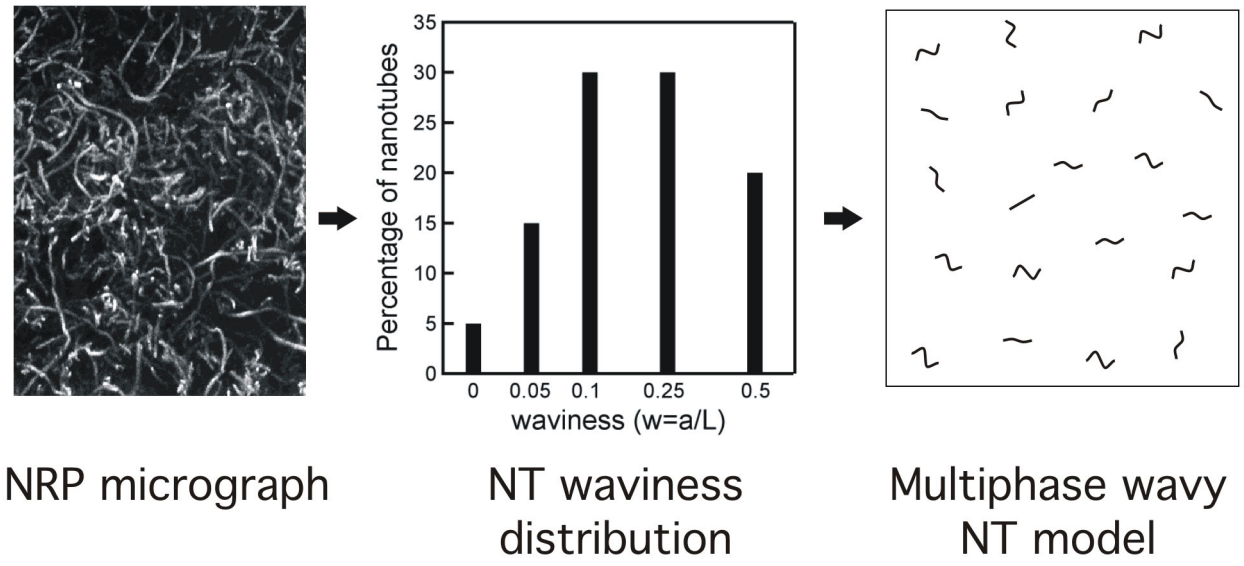

Figure 5. F. T. Fisher, R. D. Bradshaw, L. C. Brinson, "Fiber waviness in nanotube-reinforced polymer composites: I. Modulus predictions using effective nanotube properties," *Composites Science and Technology*

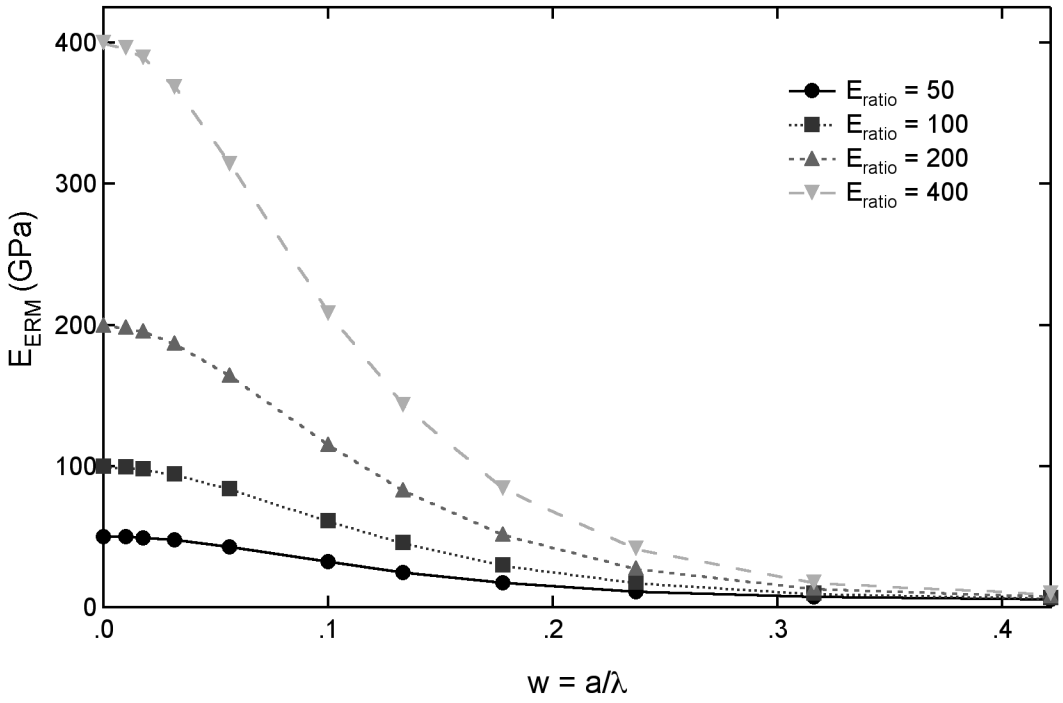

Figure 6. F. T. Fisher, R. D. Bradshaw, L. C. Brinson, "Fiber waviness in nanotube-reinforced polymer composites: I. Modulus predictions using effective nanotube properties," *Composites Science and Technology*

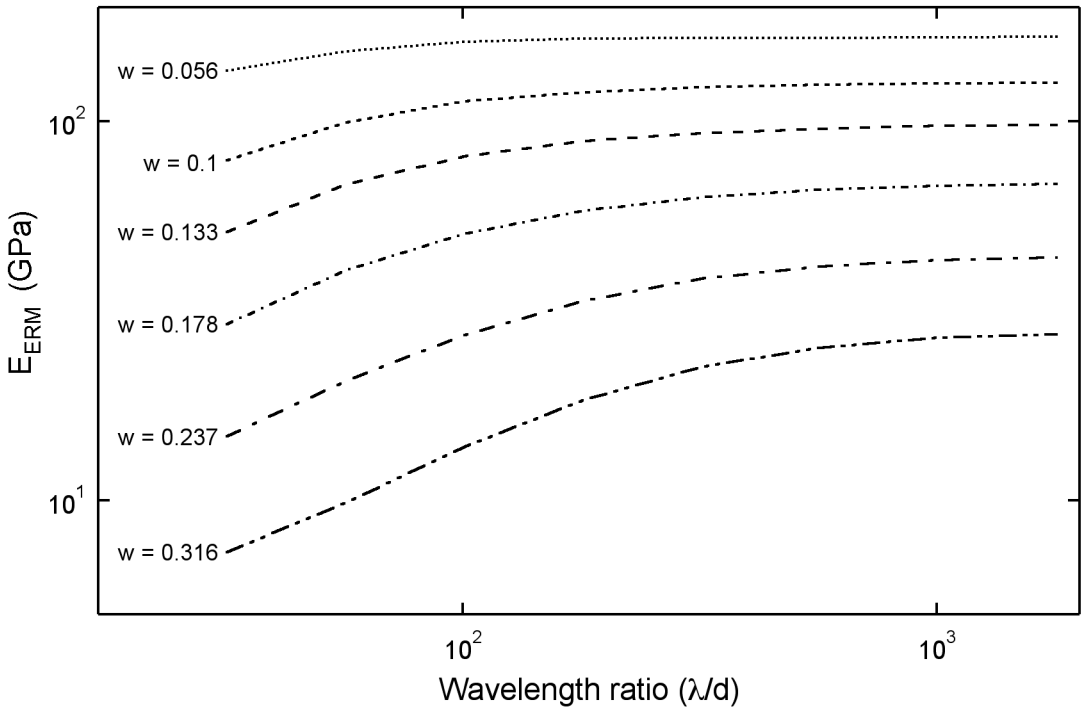

Figure 7. F. T. Fisher, R. D. Bradshaw, L. C. Brinson, "Fiber waviness in nanotube-reinforced polymer composites: I. Modulus predictions using effective nanotube properties," *Composites Science and Technology*

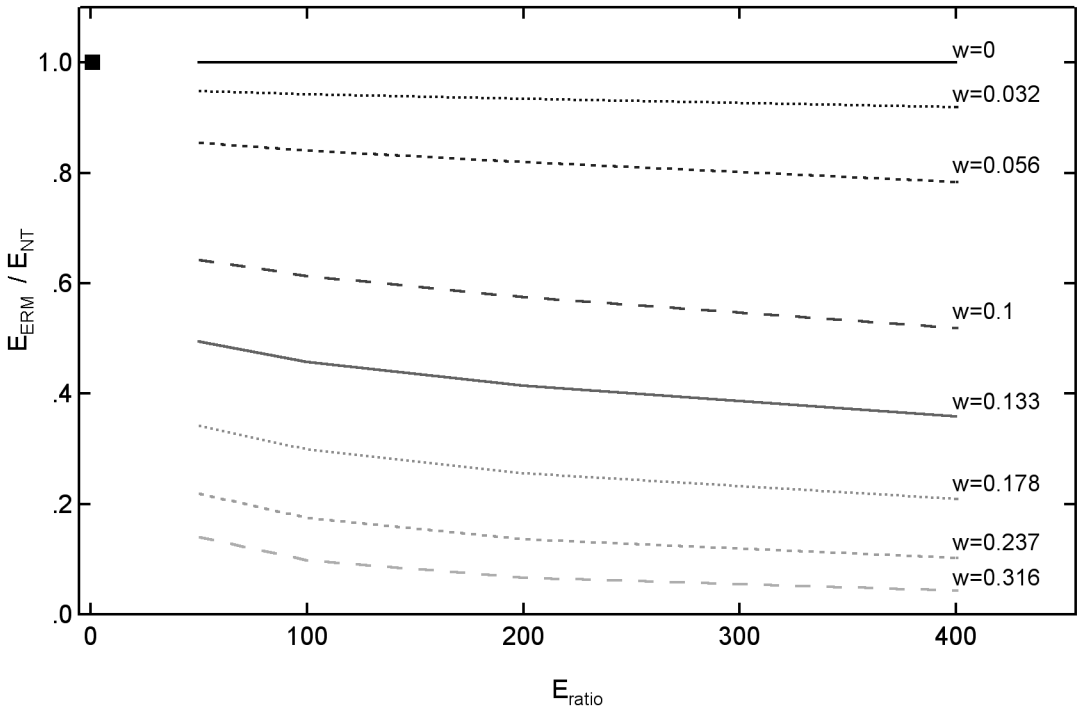

Figure 8. F. T. Fisher, R. D. Bradshaw, L. C. Brinson, "Fiber waviness in nanotube-reinforced polymer composites: I. Modulus predictions using effective nanotube properties," *Composites Science and Technology*

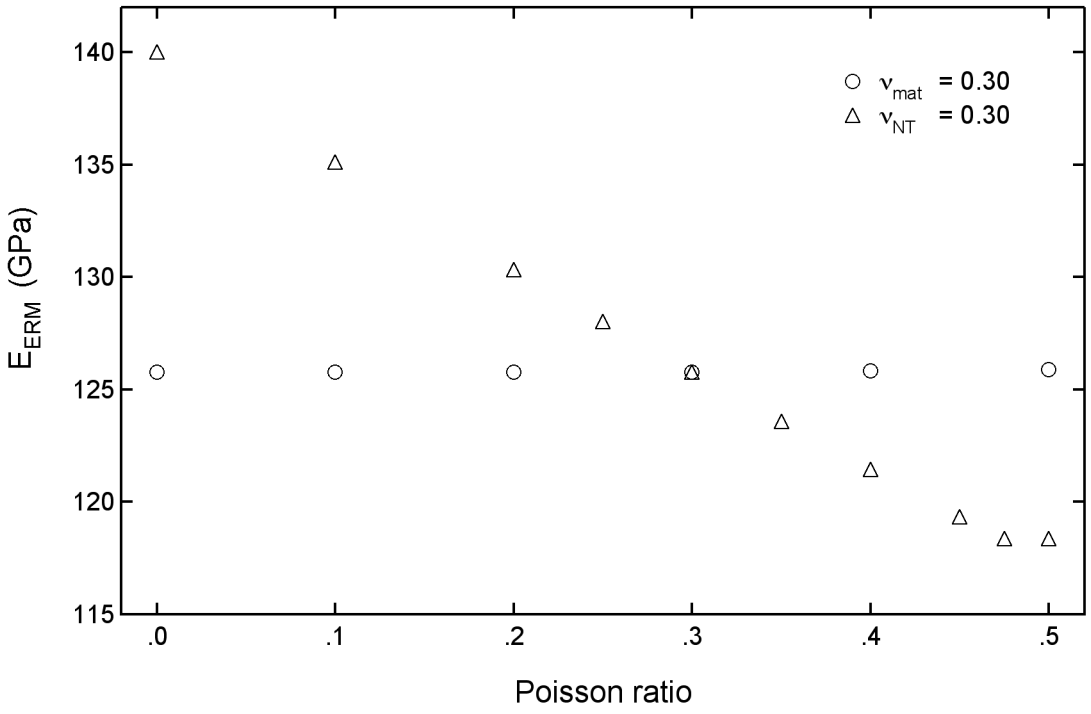

Figure 9. F. T. Fisher, R. D. Bradshaw, L. C. Brinson, "Fiber waviness in nanotube-reinforced polymer composites: I. Modulus predictions using effective nanotube properties," *Composites Science and Technology*

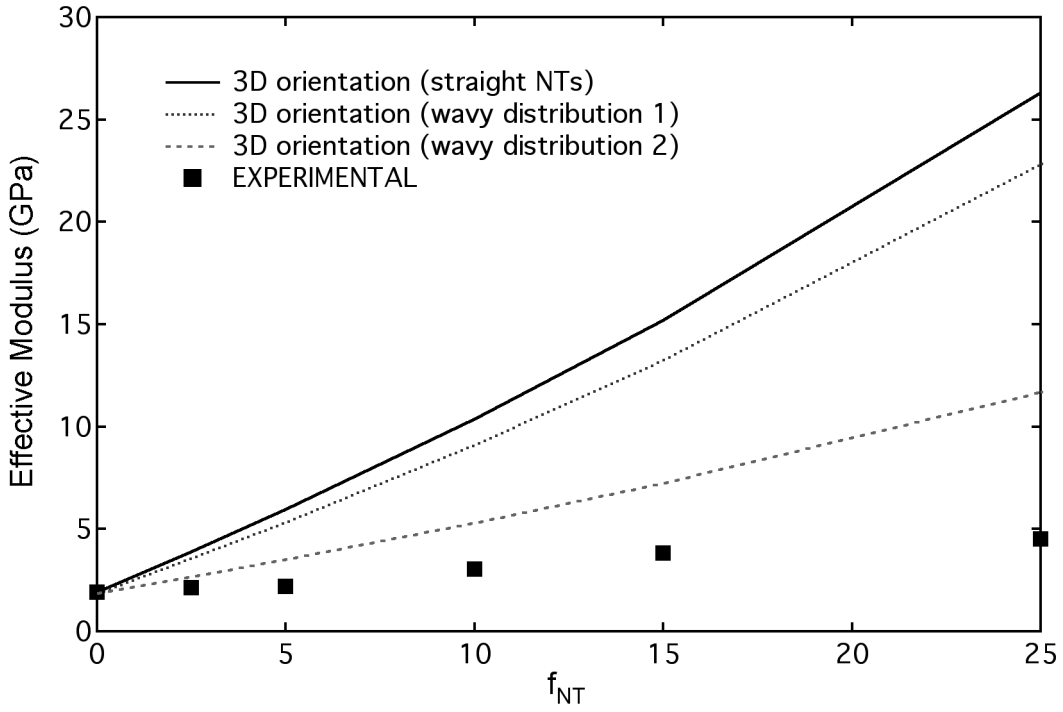

Figure 10. F. T. Fisher, R. D. Bradshaw, L. C. Brinson, "Fiber waviness in nanotube-reinforced polymer composites: I. Modulus predictions using effective nanotube properties," *Composites Science and Technology*

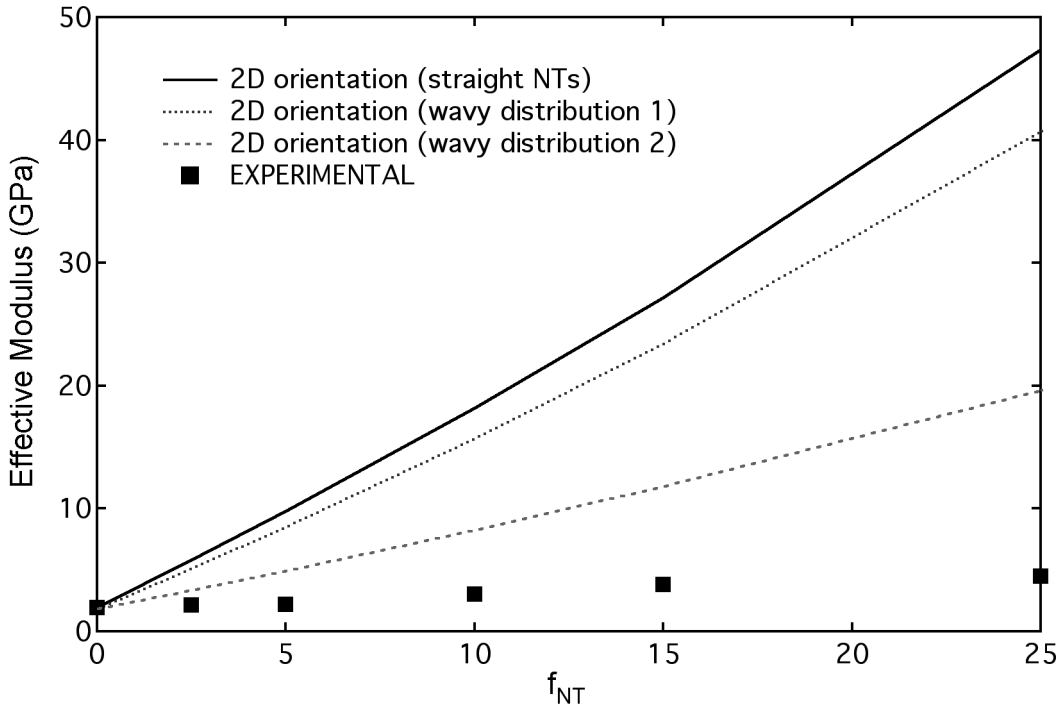

Figure 11. F. T. Fisher, R. D. Bradshaw, L. C. Brinson, "Fiber waviness in nanotube-reinforced polymer composites: I. Modulus predictions using effective nanotube properties," *Composites Science and Technology*

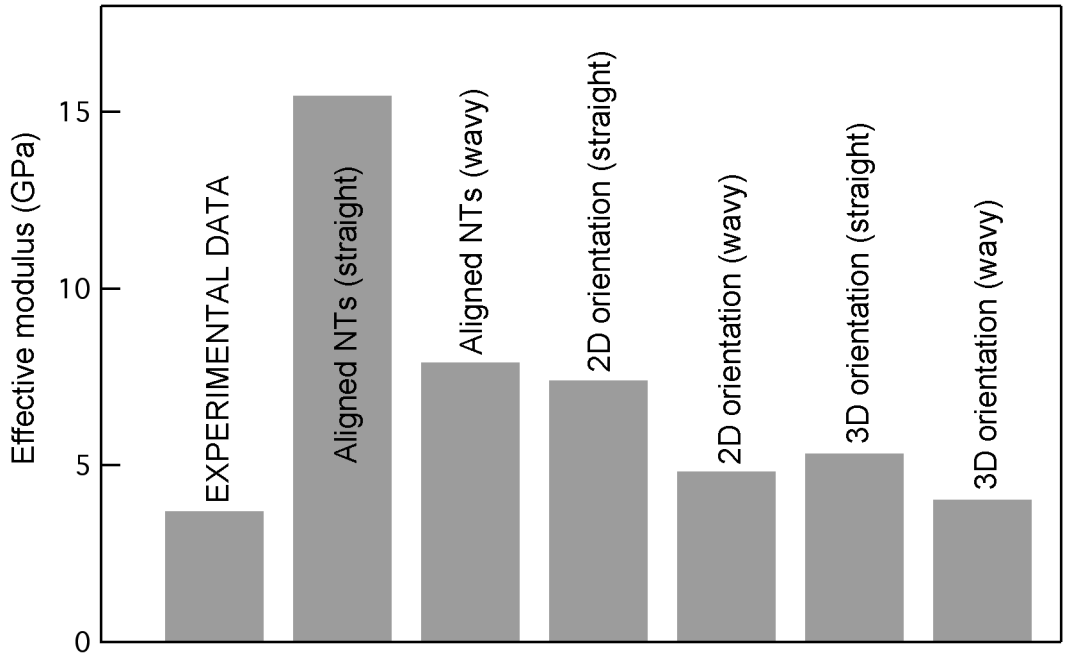

Figure 12. F. T. Fisher, R. D. Bradshaw, L. C. Brinson, "Fiber waviness in nanotube-reinforced polymer composites: I. Modulus predictions using effective nanotube properties," *Composites Science and Technology*

REFERENCES

1. Collins PG, Avouris P. Nanotubes for electronics. Scientific American 2000:December.
2. Jamieson V. Carbon nanotubes roll on. Physics World 2000;13(6).
3. Schadler LS, Giannaris SC, Ajayan PM. Load transfer in carbon nanotube epoxy composites. Applied Physics Letters 1998;73(26):3842.
4. Shaffer MSP, Windle AH. Fabrication and characterization of carbon nanotube/poly(vinyl alcohol) composites. Advanced Materials 1999;11(11):937.
5. Qian D, Dickey EC, Andrews R, Rantell T. Load transfer and deformation mechanisms in carbon nanotube-polystyrene composites. Applied Physics Letters 2000;76(20):2868.
6. Andrews R, Minot M, Jacques D, Rantell T. Processing of nanotube-polymer composites by shear mixing. Macromolecular Materials and Engineering in press.
7. Gong X, Liu J, Baskaran S, Voise RD, Young JS. Surfactant-assisted processing of carbon nanotube/polymer composites. Chemistry of Materials 2000;12:1049.
8. Demczyk BG, Cumings J, Zettl A, Ritchie RO. Structure of boron nitride nanotubules. Applied Physics Letters 2001;78(18):2772.
9. Bengu E, Marks LD. Single-walled BN nanostructures. Physical Review Letters 2001;86(11):2385.
10. Thess A, Lee R, Nikolaev P, Dia H, Petit P, Robert J, Xu C, Lee YH, Kim SG, Rinzler AG, Colbert DT, Scuseria GE, Tománek D, Fischer JE, Smalley RE. Crystalline ropes of metallic carbon nanotubes. Science 1996;273:483.
11. López MJ, Rubio A, Alonso JA, Qin L-C, Iijima S. Novel polygonized single-wall carbon nanotube bundles. Physical Review Letters 2001;86(14):3056.

12. Yu M-F, Yakobson BI, Ruoff RS. Controlled sliding and pullout of nested shells in individual multiwalled carbon nanotubes. Journal of Physical Chemistry B 2000;104:8764.

13. Gao G, Çagin T, Goddard III WA. Energetics, structure, mechanical and vibrational properties of single-walled carbon nanotubes. Nanotechnology 1998;9:184.

14. Hernández E, Goze C, Bernier P, Rubio A. Elastic properties of C and $B_xC_yN_z$ composite nanotubes. Physical Review Letters 1998;80(20):4502.

15. Che J, Çagin T, Goddard III W. Generalized extended empirical bond-order dependent force fields including nonbond interactions. Theoretical Chemistry Accounts 1999;102(346-354).

16. Sánchez-Portal S, Artacho E, Soler JM, Rubio A, Ordejón P. *Ab initio* structural, elastic, and vibrational properties of carbon nanotubes. Physical Review B 1999;59(19):12678.

17. Yakobson BI, Campbell MP, Brabec CJ, Bernholc J. High strain rate fracture and C-chain unraveling in carbon nanotubes. Computational Materials Science 1997;8:341.

18. Xin Z, Jianjun Z, Zhong-can O-Y. Strain energy and Young's modulus of single-wall carbon nanotubes calculated from electronic energy-band theory. Physical Review B 2000;62(20):13692.

19. Lu JP. Elastic properties of carbon nanotubes and nanoropes. Physical Review Letters 1997;79(7):1297.

20. Salvetat J-P, Kulik AJ, Bonard J-M, Briggs GDA, Stöckli T, Métérier K, Bonnamy S, Béguin F, Burnham NA, Forró L. Elastic modulus of ordered and disordered multiwalled carbon nanotubes. Advanced Materials 1999;11(2):161.

21. Treacy MMJ, Ebbesen TW, Gibson JM. Exceptionally high Young's modulus observed for individual carbon nanotubes. Nature 1996;381:678.

22. Krishnan A, Dujardin E, Ebbesen TW, Yianilos PN, Treacy MMJ. Young's modulus of single-walled nanotubes. Physical Review B 1998;58(20):14103.

23. Yu M-F, Files BS, Arepalli S, Ruoff RS. Tensile loading of ropes of single wall carbon nanotubes and their mechanical properties. Physical Review Letters 2000;84(24):5552.

24. Salvetat J-P, Briggs G, Bonard J-M, Basca R, Kulik A, Stöckli T, Burnham N, Forró L. Elastic and shear moduli of single-walled carbon nanotube ropes. Physical Review Letters 1999;82(5):944.

25. Wong EW, Sheehan PE, Lieber CM. Nanobeam mechanics: Elasticity, strength, and toughness of nanorods and nanotubes. Science 1997;277:1971.

26. Poncharal P, Wang ZL, Ugarte D, de Heer WA. Electrostatic deflections and electromechanical resonances of carbon nanotubes. Science 1999;283:1513.

27. Yu M-F, Lourie O, Dyer M, Moloni K, Kelly TF, Ruoff RS. Strength and breaking mechanism of multiwalled carbon nanotubes under tensile load. Science 2000;287:637.

28. Ajayan P, Stephan O, Colliex C, Trauth D. Aligned carbon nanotube arrays formed by cutting a polymer resin-nanotube composite. Science 1994;265:1212.

29. Jin L, Bower C, Zhou O. Alignment of carbon nanotubes in a polymer matrix by mechanical stretching. Applied Physics Letters 1998;73(9):1197.

30. Bower C, Rosen R, Lin J, Han J, Zhou O. Deformation of carbon nanotubes in nanotube-polymer composites. Applied Physics Letters 1999;74(22):3317.

31. Haggenmueller R, Gommans HH, Rinzler AG, Fischer JE, Winey KI. Aligned single-wall carbon nanotubes in composites by melt processing methods. Chemical Physics Letters 2000;330:219.

32. Smith BW, Benes Z, Luzzi DE, Fischer JE, Walters DA, Casavant MJ, Schmidt J, Smalley RE. Structural anisotropy of magnetically aligned single wall carbon nanotube films. Applied Physics Letters 2000;77(5):663.

33. Jia Z, Wang Z, Xu C, Liang J, Wei B, Wu D, Zhu S. Study on poly(methly methacrylate)/carbon nanotube composites. Materials Science and Engineering A 1999;271:395.

34. Ajayan PM, Schadler LS, Giannaris C, Rubio A. Single-walled carbon nanotube-polymer composites: Strength and weakness. Advanced Materials 2000;12(10):750.

35. Lordi V, Yao N. Molecular mechanics of binding in carbon-nanotube-polymer composites. Journal of Materials Research 2000;15(12):2770.

36. Lozano K, Barrera E. Nanofiber-reinforced thermoplastic composites. I. Thermoanalytical and mechanical analyses. Journal of Applied Polymer Science 2001;79:125.

37. Stéphan C, Nguyen TP, de la Chapelle ML, Lefrant S, Journet C, Bernier P. Characterization of singlewalled carbon nanotubes-PMMA composites. Synthetic Metals 2000;108:139.

38. Lourie O, Wagner HD. Transmission electron microscopy observations of fracture of single-wall carbon nanotubes under axial tension. Applied Physics Letters 1998;73(24):3527.

39. Srivastava D, Brenner DW, Schall JD, Ausman KD, Yu M-F, Ruoff RS. Predictions of enhanced chemistry reactivity at regions of local conformational strain on carbon nanotubes: Kinky chemistry. Journal of Physical Chemistry B 1999;103(21):4330.

40. Wagner HD, Lourie O, Feldman Y, Tenne R. Stress-induced fragmentation of multiwall carbon nanotubes in a polymer matrix. Applied Physics Letters 1998;72(2):188.

41. Fisher FT, Bradshaw RD, Brinson LC. Effects of nanotube waviness on the modulus of nanotube-reinforced polymers. Applied Physics Letters 2002;80(24).

42. Yakobson BI, Smalley RE. Fullerene nanotubes: $C_{1,000,000}$ and beyond. American Scientist 1997;July-August.

43. Ruoff RS, Lorents DC. Mechanical and thermal properties of carbon nanotubes. Carbon 1995;33(7):925.

44. Govindjee S, Sackman J. On the use of continuum mechanics to estimate the properties of nanotubes. Solid State Communications 1999;111:227.

45. Bradshaw RD, Fisher FT, Brinson LC. Fiber waviness in nanotube-reinforced polymer composites: II. Modelling via numerical approximation of the dilute strain concentration tensor. Composites Science and Technology 2002:submitted.

46. Mori T, Tanaka K. Average stress in matrix and average elastic energy of materials with misfitting inclusions. Acta Metallurgica 1973;21:571.

47. Benveniste Y. A new approach to the application of Mori-Tanaka's theory in composite materials. Mechanics of Materials 1987;6:147.

48. Weng GJ. The theoretical connection between Mori-Tanaka's theory and the Hashin-Shtrikman-Wadpole bounds. International Journal of Engineering Science 1990;28(11):1111.

49. Zhao YH, Weng GJ. Effective elastic moduli of ribbon-reinforced composites. Journal of Applied Mechanics 1990;57:158.

50. Qui YP, Weng GJ. The influence of inclusion shape on the overall elastoplastic behavior of a two-phase isotropic composite. International Journal of Solids and Structures 1991;27(12):1537.

51. Brinson L, Lin W. Comparison of micromechanics methods for effective properties of multiphase viscoelastic composites. Composite Structures 1998;41:353.

52. Fisher FT, Brinson LC. Viscoelastic interphases in polymer matrix composites: Theoretical models and finite element analysis. Composites Science and Technology 2001;61(5):731.

53. Tandon GP, Weng GJ. Average stress in the matrix and effective moduli of randomly orientated composites. Composites Science and Technology 1986;27:111.

54. Fisher FT. Nanomechanics of carbon nanotube-reinforced polymers. Northwestern University, Evanston, IL, 2002.

55. Odegard G, Gates T, Nicholson L, Wise K. Equivalent-continuum modeling of nano-structured materials. TM-2001-210863. Hampton, VA: NASA, 2001.

56. Andrews R, Jacques D, Rao AM, Derbyshire F, Qian D, Fan X, Dickey EC, Chen J. Continuous production of aligned carbon nanotubes: A step closer to commercial realization. Chemical Physics Letters 1999;303(16):467.

57. Andrews R. Personal communication.

58. Pan ZW, Xie SS, Lu L, Chang BH, Sun LF, Zhou WY, Wang G, Zhang DL. Tensile tests of ropes of very long aligned multiwalled carbon nanotubes. Applied Physics Letters 1999;74(21):3152.

59. Jin Z, Pramoda K, Xu G, Goh S. Dynamic mechanical behavior of melt-processed multi-walled carbon nanotube/poly(methyl methacrylate) composites. Chemical Physics Letters 2001;37:43.

60. Fox RW, McDonald AT. Introduction to fluid mechanics. 4th ed. New York: John Wiley & Sons, Inc, 1992.

61. Mura T. Micromechanics of defects in solids. 2nd ed. Dordrecht: Kluwer Academic Publishers, 1982.